Supporting Information

Three-Dimensional, Hetero-structured, Cu_3P@C Nanosheets with Excellent Cycling Stability as Na-ion Battery Anode Material

Jinliang Zhu[a,*], Qiuchen He[a], Yang Liu[a], Julian Key[a], Shuangxi Nie[b], Mingmei Wu[c] and Pei Kang Shen[a,*]

[a] Collaborative Innovation Center of Sustainable Energy Materials, School of Resources, Environment and Materials, Guangxi University, 100 Daxue Dong Road, Nanning 530004, PR China.

[b] Guangxi Key Laboratory of Clean Pulp & Papermaking and Pollution Control, Guangxi University, 100 Daxue Dong Road, Nanning 530004, PR China.

[c] School of Chemistry, Sun Yat-sen University, Guangzhou 510275, PR China.

[*] Corresponding author. E-mail: jlzhu@163.com (Jinliang Zhu), stsspk@mail.sysu.edu.cn (Pei Kang Shen), Fax: +86 07713237990, Tel: +86 07713237990.

Table S1. The main synthesis methods of copper phosphides reported in literatures

Copper phosphide	Mophology	Synthesis	Phosphorus source and precursor	Ref.
Cu_3P	Amorphous form	Solid state synthesis	Red phosphorus + Cu (or electrodeposited copper)	[S1] [S2]
Cu_3P	Powder	Solvothermal synthesis	White phosphorus + $CuCl_2{\cdot}2H_2O$	[S3]
Cu_3P	Particle	Solvothermal synthesis	Red phosphorus + $CuCl_2{\cdot}2H_2O$	[S4]
Cu_3P	Aggregated nanoparticle	Solvothermal synthesis	Yellow phosphorus + $CuCl_2{\cdot}2H_2O$	[S5]
Cu_3P	Polydispersed particle	Solvothermal synthesis	White phosphorus + Prepared Cu nanoparticle	[S6]
Cu_3P	Nanorod	Solvothermal synthesis	Yellow phosphorus + $CuCl_2{\cdot}2H_2O$	[S7]
Cu_3P	Nanopillar	Solid–vapor reaction	Red phosphorus + Electrodeposited Cu nanorod	[S8]
Cu_3P	Powder	Ball milling	Red phosphorus + Copper powder	[S9]
Cu_3P	Powder	Solid-state reaction	Red phosphorus + Cu	[S10-S12]
Cu_3P	Micronic sphere	Solvothermal synthesis	Yellow phosphorus+ $CuSO_4{\cdot}5H_2O$ or $Cu(OH)_2$	[S13] [S14]
Cu_3P	Sheet-like nanocrystalline	Hydrothermal synthesis	Yellow phosphorous + $CuCl_2{\cdot}2H_2O$	[S15]
Cu_3P	Platelet	Solvothermal synthesis	PH_3 gas + CuCl	[S16]
Cu_3P	Nanowire	Thermal decomposition	Sodium hypophosphite + $Cu(OH)_2$ nanowire	[S17]
Cu_3P	Plate-like nanocrystal	Solvothermal using standard Schlenk line	TOPO, TOP + CuCl	[S18] [S19]
Cu_3P/Cu	Aggregated particle	High temperature reaction	Red phosphorus + Cu foam	[S20]
CuP_2	Nanoparticle	Solvothermal synthesis	White phosphorus + prepared Cu nanoparticle	[S21]
CuP_2	Textured powder	Solid-state reaction	White phosphorus + $CuCl_2$	[S22]
CuP_2	Particle	Ball milling	Red phosphorus + Copper powder	[S23]
Cu_3P	Nanosheet	Heat treatment	P-containing resin + Cu foam	This work

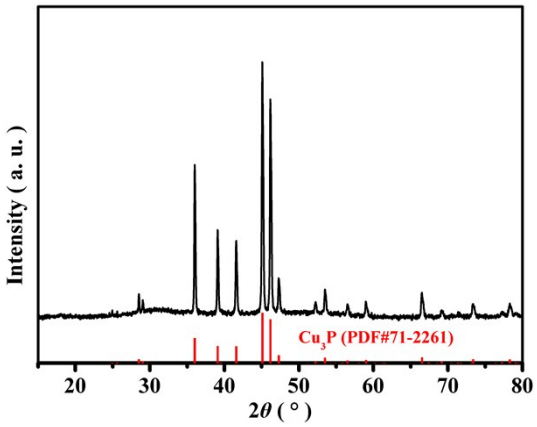

Fig. S1 XRD pattern of Cu_3P powder.

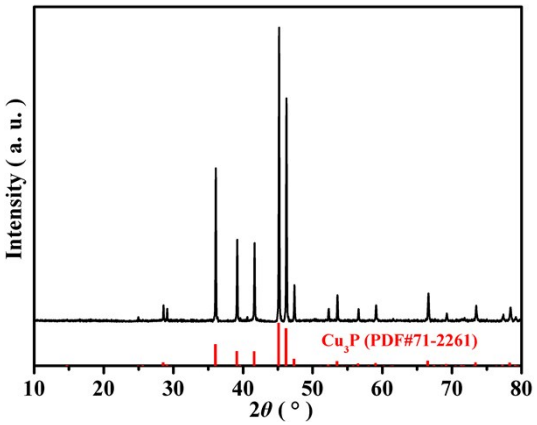

Fig. S2 XRD pattern of Cu_3P/C.

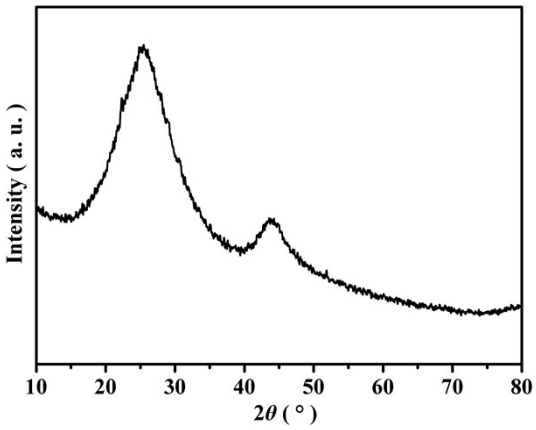

Fig. S3 XRD pattern of C^P.

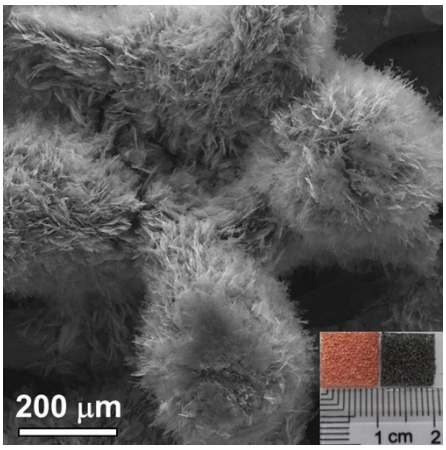

Fig. S4 SEM image of Cu_3P@C5.

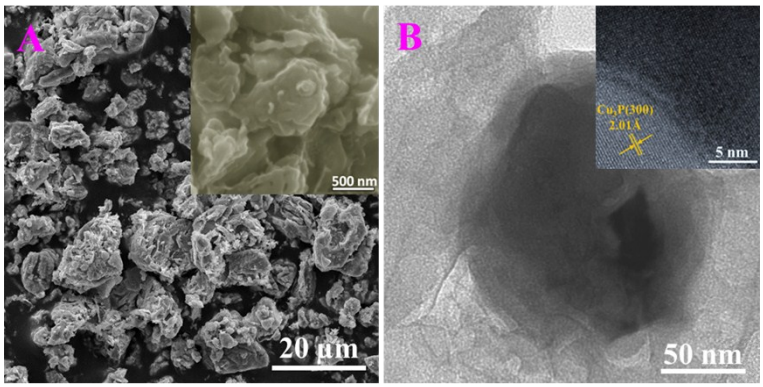

Fig. S5 SEM and TEM images of Cu_3P powder.

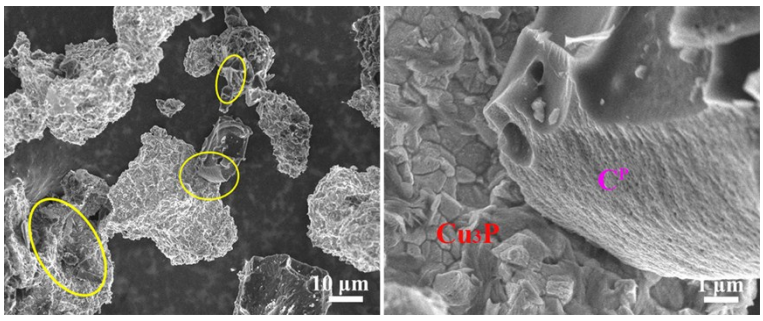

Fig. S6 SEM images of Cu_3P/C

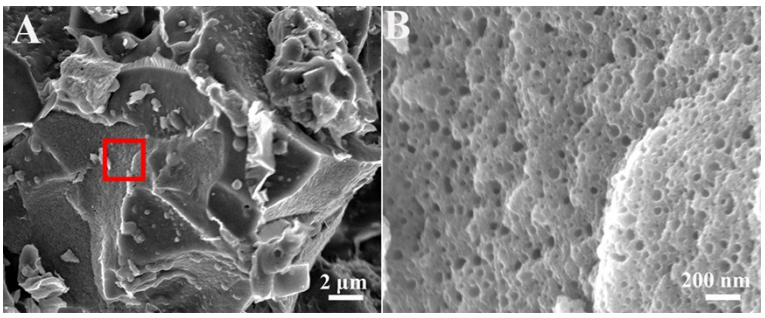

Fig. S7 SEM images of C^P

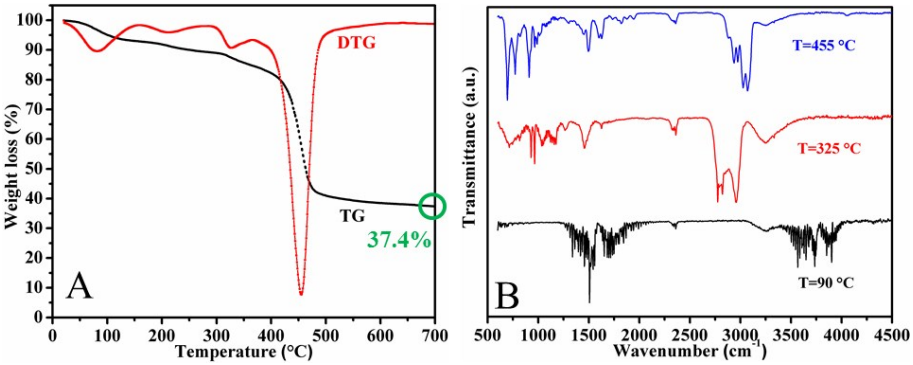

Fig. S8 (A) TG-DTG of the resin in N_2 from 25 °C to 800 °C and (B) FTIR spectra of the corresponding pyrolysis products at 90, 325 and 455 °C, respectively.

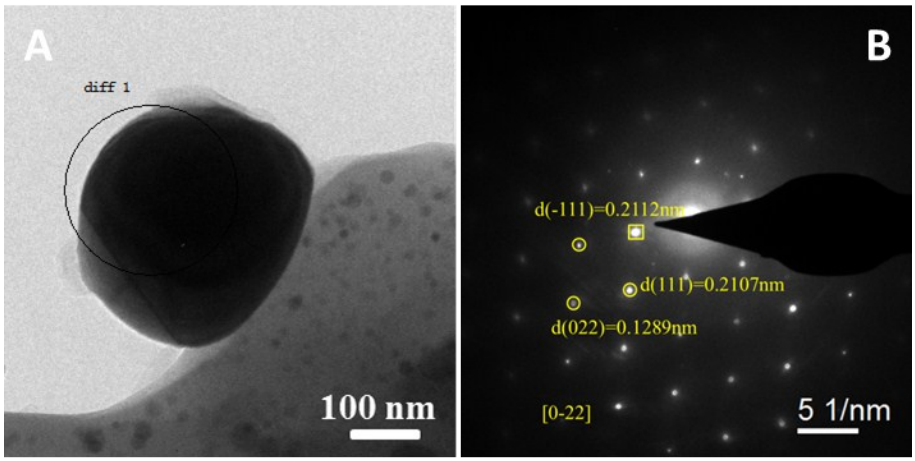

Fig. S9 (A) TEM image and (B) selected-area electron diffraction of a sphere-like Cu particles.

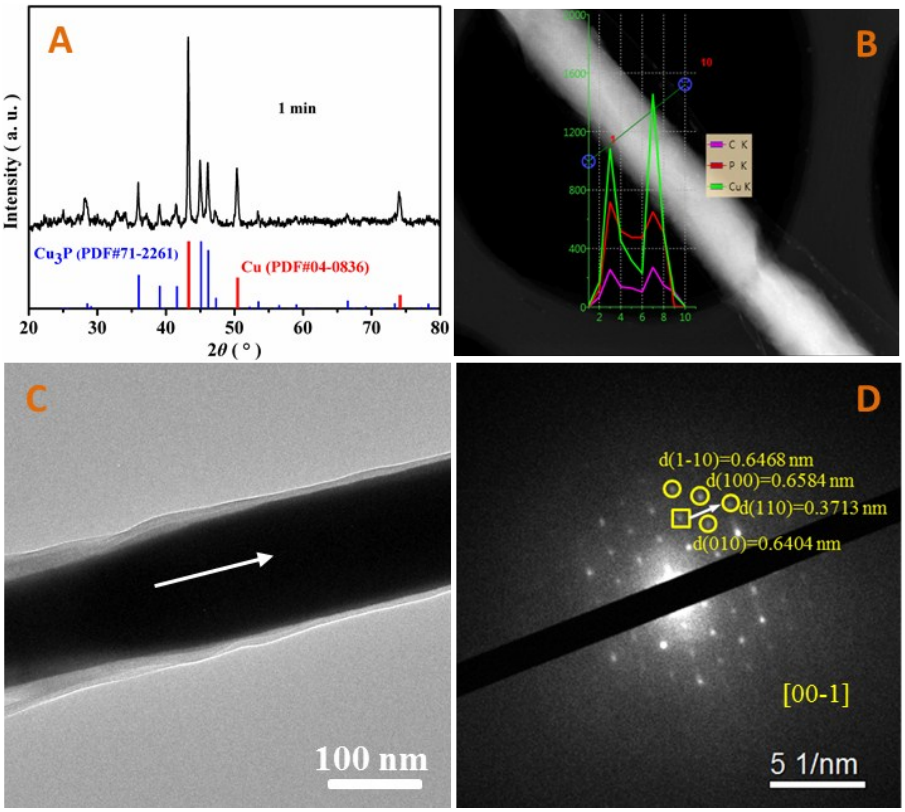

Fig. S10 (A) XRD pattern, (B) EDS line scanning curve, (C) TEM image and (D) selected-area electron diffraction of a single nanobelt at 900 °C 1 min.

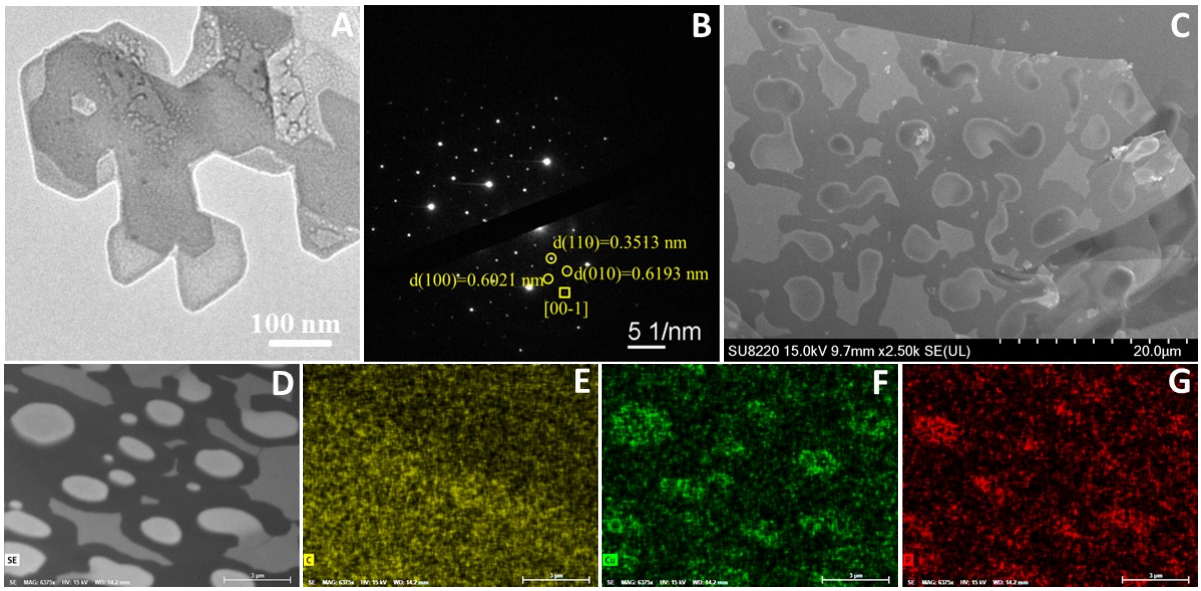

Fig. S11 (A) TEM image, (B) selected-area electron diffraction, (C, D) SEM image and (E) C mapping, (F) Cu mapping and (G) P mapping of a growing nanosheet at 900 °C 30 min.

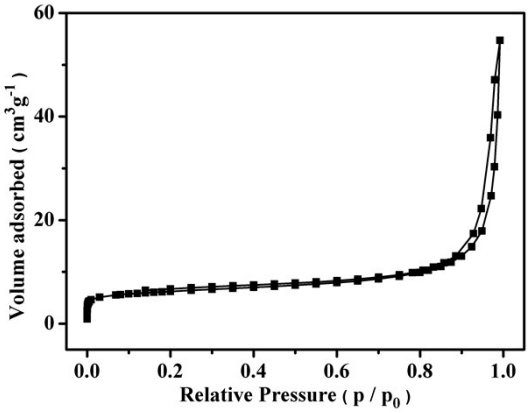

Fig. S12 N_2 adsorption-desorption isotherm of Cu_3P@C5.

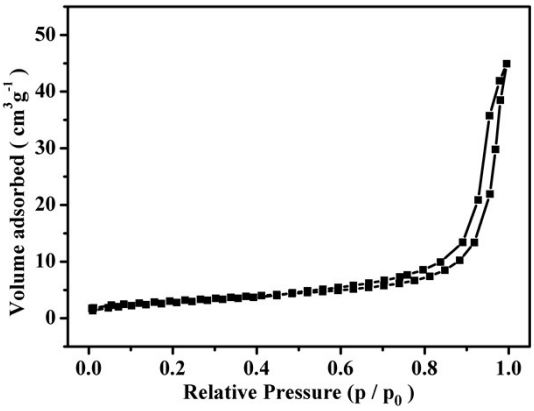

Fig. S13 N_2 adsorption-desorption isotherm of Cu_3P@C15.

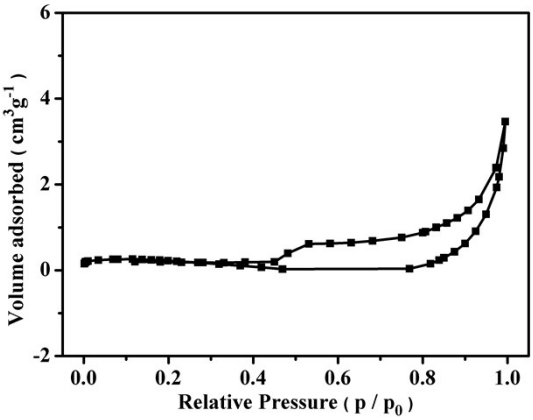

Fig. S14 N_2 adsorption-desorption isotherm of Cu_3P powder.

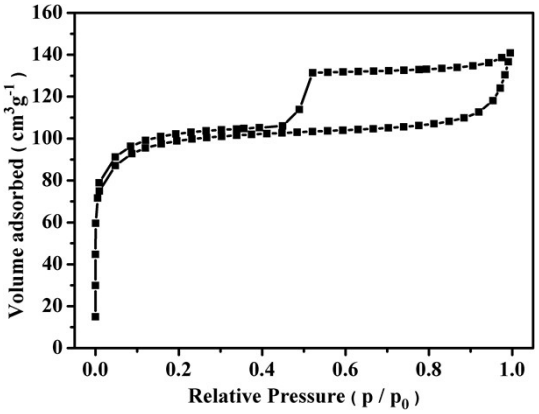

Fig. S15 N_2 adsorption-desorption isotherm of C^P.

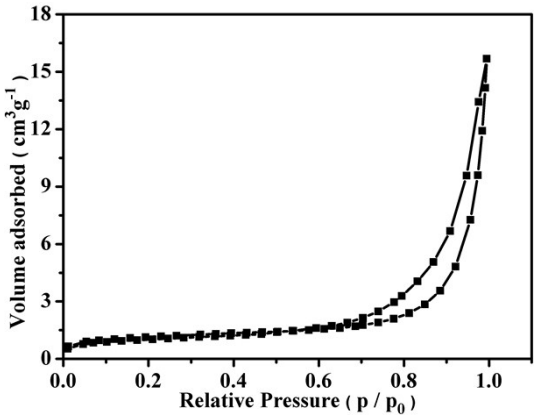

Fig. S16 N_2 adsorption-desorption isotherm of Cu_3P/C.

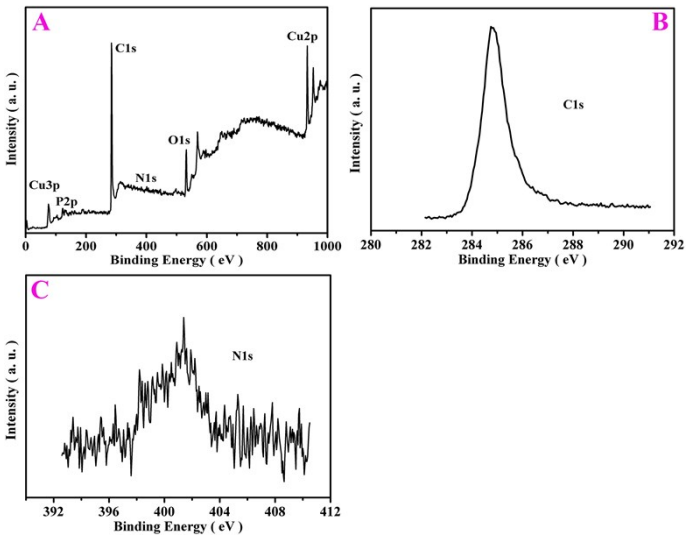

Fig. S17 XPS spectrum (A), XPS-C1s (B) and XPS-N1s (C) of Cu_3P@C5

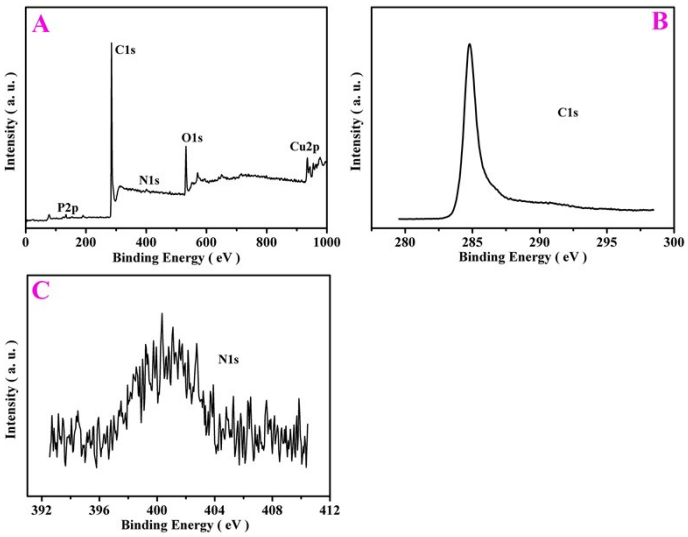

Fig. S18 XPS spectrum (A), XPS-C1s (B) and XPS-N1s (C) of Cu_3P@C15

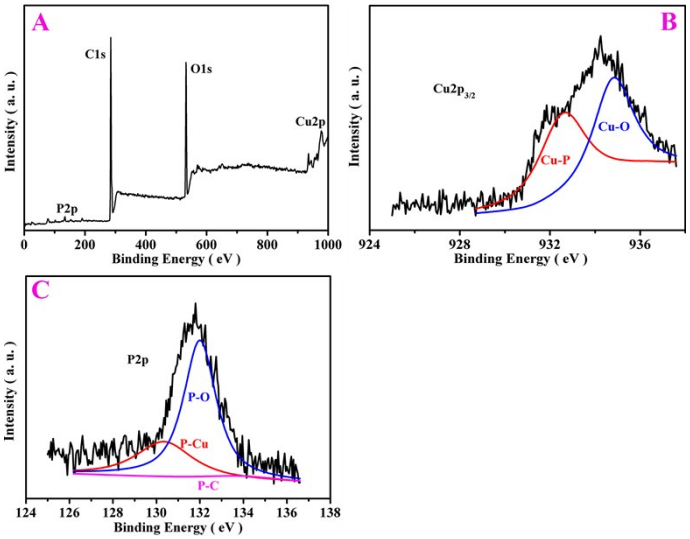

Fig. S19 XPS spectrum (A), XPS-$Cu2p_{3/2}$ (B) and XPS-P2p (C) of Cu_3P powder

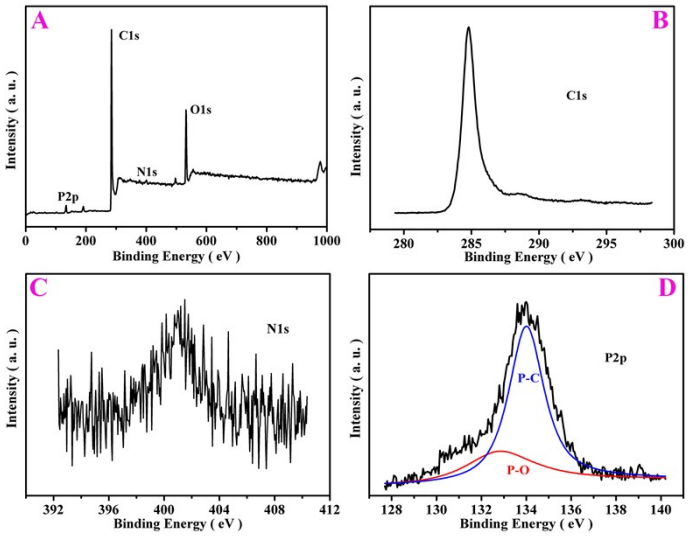

Fig. S20 XPS spectrum (A), XPS-C1s (B), XPS-N1s (C) and XPS-P2p (D) of C^P

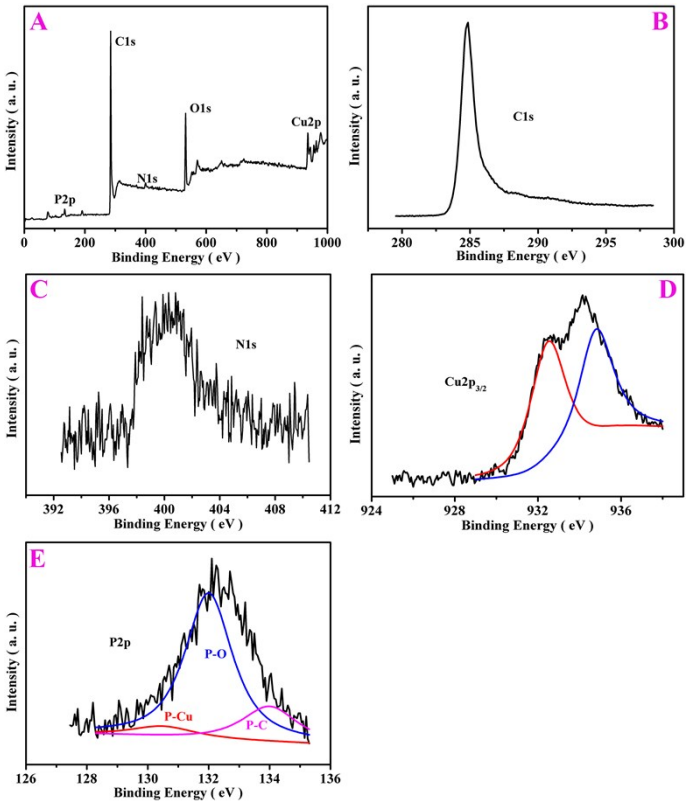

Fig. S21 XPS spectrum (A), XPS-C1s (B), XPS-N1s (C), XPS-Cu2$p_{3/2}$ (D) and XPS-P2p (E) of Cu_3P/C

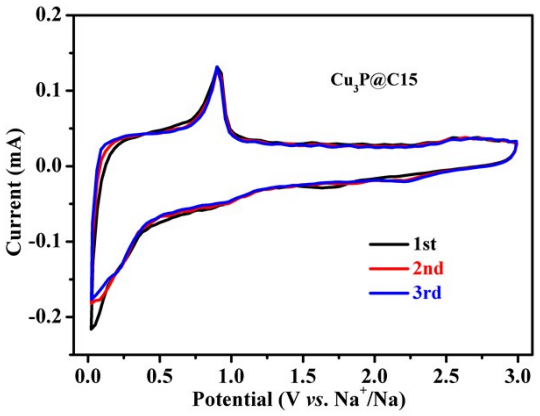

Fig. S22 Cyclic voltammogram **(**CV) curves of Cu_3P@C15 at 0.1 mV s^{-1} between 0.01 and 3.0 V *vs.* Na^+/Na.

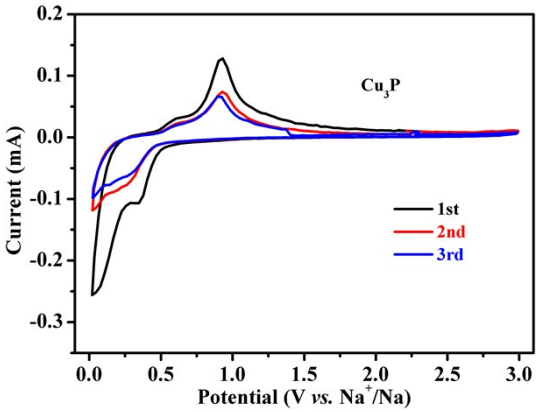

Fig. S23 CV curves of Cu_3P powder at 0.1 mV s^{-1} between 0.01 and 3.0 V *vs.* Na^+/Na.

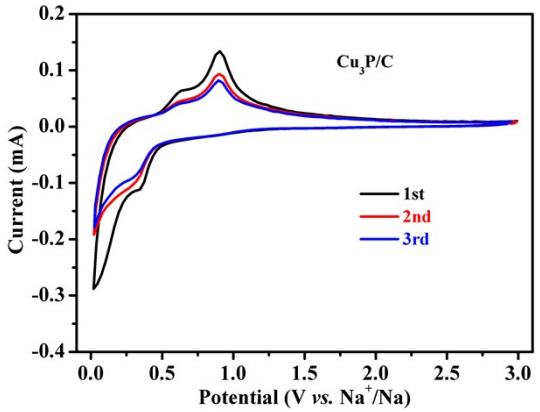

Fig. S24 CV curves of Cu_3P/C at 0.1 mV s^{-1} between 0.01 and 3.0 V *vs.* Na^+/Na.

Table S2. Comprehensive overview of recently reported metal phosphide-based SIB electrode materials.

Metal phosphide	Synthesis method	Discharge current (mA g^{-1})	Cycle number	Discharge capacities (2^{nd} cycle to final cycle mAh g^{-1})	Decay capacity per cycle (mAh g^{-1})	Decay ratio per cycle (%)
Cu_3P/CNS[S24]	Solid state synthesis	1000	100	～176 to 151	0.250	0.142%
Cu_3P(CPNW) [S17]	Thermal decomposition	1000	260	196 to 134	0.238	0.122%
CuP_2/C[S25]	Ball milling	200	100	～450 to ～430	0.200	0.044%
CuP_2/C[S23]	Ball milling	150	30	～450 to ～430	0.667	0.347%
CuP_2/C [S26]	Ball milling	500	200	～550 to 379	0.855	0.155%
Cu_3P-Co_2P [S27]	Electrospinning	5000	2000	～600 to 317	0.142	0.024%
FeP(FePNC) [S28]	Thermal decomposition	200	200	～293 to 275	0.090	0.031%
FeP/NPG [S29]	Thermal decomposition	1000	700	422 to 378	0.063	0.015%
CNT@FeP@C[S30]	Thermal decomposition	500	500	328 to 295	0.066	0.013%
H-FeP@C@GR[S31]	Thermal decomposition	100	250	～730 to 400	1.320	0.181%
CoP/FeP[S32]	Thermal decomposition	100	200	～653 to 456	0.985	0.151%
Co_2P-3D PNC[S33]	Thermal decomposition	500	700	～360 to 271	0.127	0.035%
A-Co_2P/$C_xN_yB_z$ -650[S34]	Solid state synthesis	200	100	251 to 217	0.340	0.135%
CoP@C-RGO-NF[S35]	Thermal decomposition	100	100	～910 to 473	4.370	0.480%
CoP@DC@GR[S36]	Thermal decomposition	500	200	569 to 398	0.855	0.150%
CoP_3@C[S37]	Ball milling	300	260	～240 to 146	0.362	0.151%
$Ni_{1.5}Co_{1.5}P_x$ [S38]	Thermal decomposition	1C	100	600 to ～189	4.110	0.685%
Ni_2P@C [S39]	Thermal decomposition	50	100	～380 to 296	0.840	0.221%

Ni_2P@NPC [S40]	Solid state synthesis	500	1200	～240 to 181	0.049	0.020%
Ni_2P/NG/Ni_2P [S41]	Thermal decomposition	1000	400	～225 to 108	0.295	0.131%
Ni_2P⊂pGN [S42]	Solid state synthesis	200	100	～270 to 161	1.090	0.404%
Ni_2P/3DG-8 [S43]	Thermal decomposition	1000	100	～850 to 230	6.200	0.729%
Ni_2P@C/GA[S44]	Thermal decomposition	1000	2000	～400 to 125	0.138	0.034%
V_4P_7 /5P[S45]	Ball milling	500	100	613 to 294	3.190	0.520%
Cu_4SnP_{10}/MWCNTs [S46]	Solvothermal synthesis	1000	100	～600 to 325	2.75	0.458%
$MGeP_x$ [S47]	Solid state synthesis	1200	200	～1100 to 278	4.110	0.374%
WP/CC [S48]	Thermal decomposition	2000	1000	～300 to 50	0.250	0.083%
Sn_4P_3 /GA-2 [S49]	Thermal decomposition	100	100	～820 to 657	1.630	0.199%
Sn_4P_3@C [S50]	Thermal decomposition	100	120	～780 to 700	0.667	0.085%
Sn_4P_3@C [S51]	Solvothermal synthesis	1500	400	～670 to 360	0.775	0.116%
Sn_4P_3 [S52]	Solvothermal synthesis“	200	250	480 to 303	0.708	0.148%
Sn_4P_3@C [S53]	Solvothermal synthesis	2000	500	726 to 368	0.716	0.099%
Sn_4P_3–C [S54]	Solvothermal synthesis	2000	2000	～700 to 420	0.140	0.020%
Sn_4P_3[S55]	Solution-Liquid- Solid Growth	500	80	488 to 400	1.100	0.225%
Sn_4P_3/RGO [S56]	Solvothermal	1000	1500	～690 to 362	0.219	0.032%
Sn_4P_3 [S57]	Solvothermal	100	100	～570 to 473	0.970	0.170%
Sn_4P_3(SPPG) [S58]	Ball milling	2000	1000	561 to 371	0.190	0.034%
Cu_3P@C5 (this work)	Epitaxial phosphidation growth	5000	2000	162 to 118	0.022	0.013%

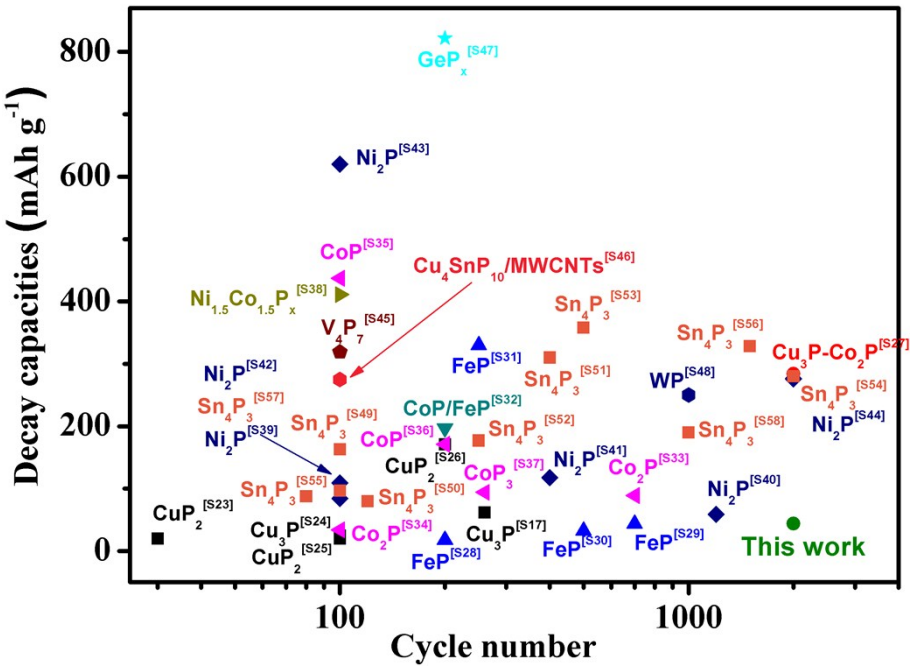

Fig. S25 Decay capacities of metal phosphide-based SIB electrode materials recently reported in the literature (within Fig. "This work" in green text refers to Cu_3P@C5).

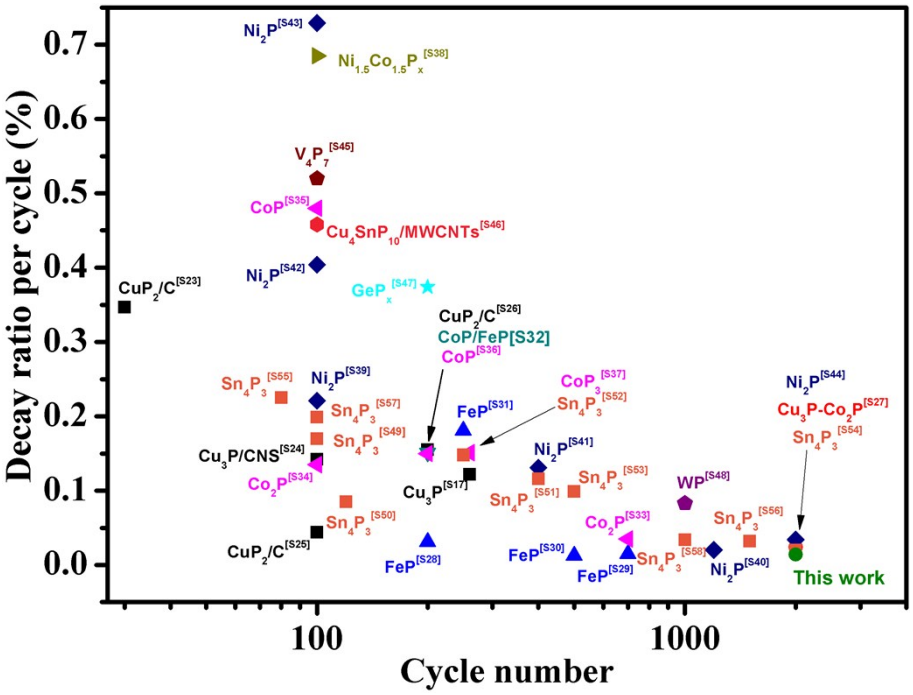

Fig. S26 Capacity decay ratio per cycle of metal phosphide-based SIB electrode materials recently reported in the literature (within Fig. "This work" in green text refers to Cu_3P@C5).

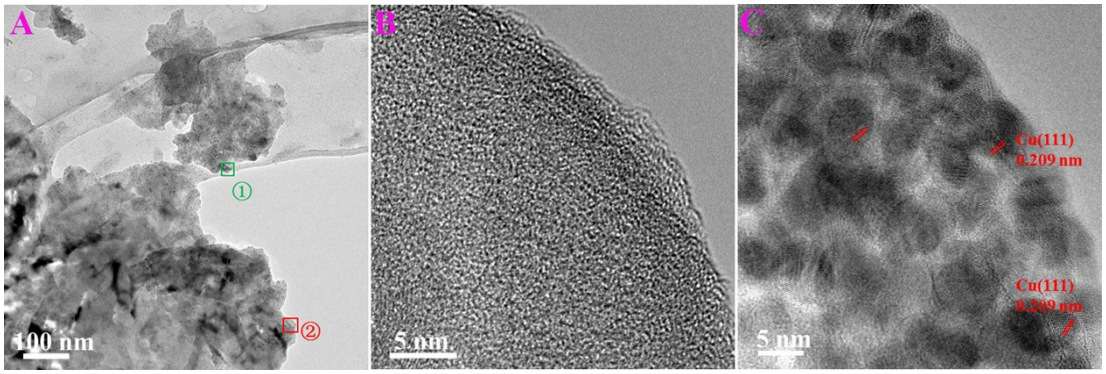

Fig. S27 TEM images of Cu_3P/C after 300 cycles.

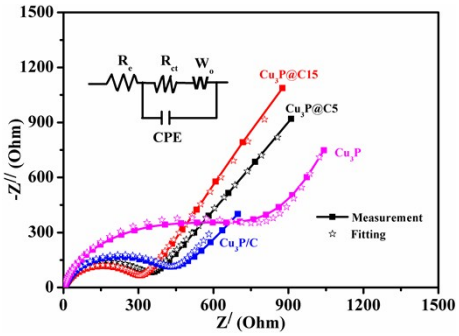

Fig. S28 EIS spectra and equivalent circuit of Cu_3P@C5, Cu_3P@C15, Cu_3P/C and Cu_3P. (Where R_e, R_{ct}, CPE, and W_o in the fitted equivalent circuit are electrolyte resistance, charge-transfer resistance at the electrode/electrolyte interface, constant phase element impedance, and Warburg impedance, respectively.)

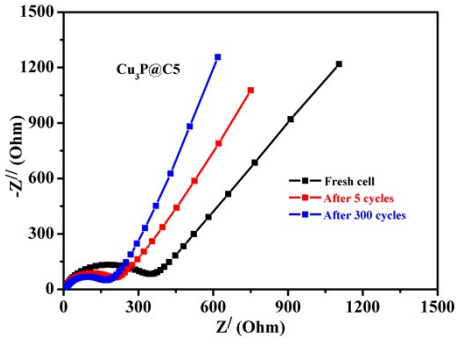

Fig. S29 EIS spectra of Cu_3P@C5 before cycling and after different cycles in a fully charged state.

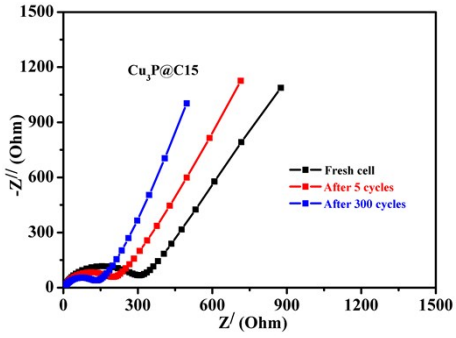

Fig. S30 EIS spectra of Cu_3P@C15 before cycling and after different cycles in a fully charged state.

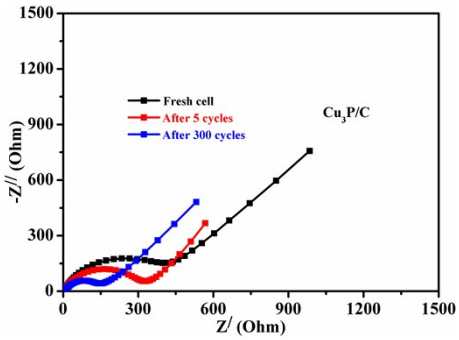

Fig. S31 EIS spectra of Cu_3P/C before cycling and after different cycles in a fully charged state.

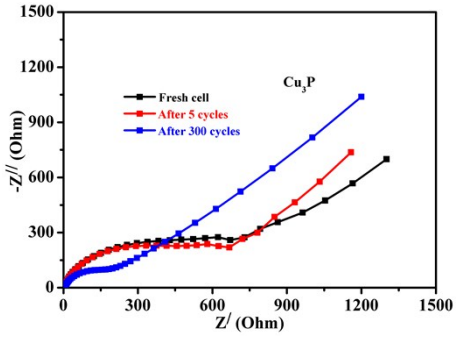

Fig. S32 EIS spectra of Cu_3P before cycling and after different cycles in a fully charged state.

References

[S1] B. Mauvernay, M. L. Doublet and L. Monconduit, *Journal of Physics and Chemistry of Solids*, **2006**, 67, 1252.

[S2] M. Chandrasekar and S. Mitra, *Electrochimica Acta*, **2013**, 92, 47.

[S3] M.-P. Bichat, T. Politova, H. Pfeiffer, F. Tancret, L. Monconduit, J.-L. Pascal, T. Brousse and F. Favier, *Journal of Power Sources*, **2004**, 136, 80.

[S4] M. Bichat, T. Politova, J. Pascal, F. Favier and L. Monconduit, *Journal of The Electrochemical Society*, **2004**, 151, A2074.

[S5] Y. Xie, H. Su, X. Qian, X. Liu and Y. Qian, *Journal of Solid State Chemistry*, **2000**, 149, 88.

[S6] S. Carenco, Y. Hu, I. Florea, O. Ersen, C. Boissière, N. Mézailles and C. Sanchez, *Chemistry of Materials*, **2012**, 24, 4134.

[S7] Z. Sun, Q. Yue, J. Li, J. Xu, H. Zheng and P. Du, *Journal of Materials Chemistry A*, **2015**, 3, 10243.

[S8] C. Villevieille, F. Robert, P. L. Taberna, L. Bazin, P. Simon and L. Monconduit, *Journal of Materials Chemistry*, **2008**, 18, 5956.

[S9] M. C. Stan, R. Klöpsch, A. Bhaskar, J. Li, S. Passerini and M. Winter, *Advanced Energy Materials*, **2013**, 3, 231.

[S10] H. Pfeiffer, F. Tancret, M.-P. Bichat, L. Monconduit, F. Favier and T. Brousse, *Electrochemistry communications*, **2004**, 6, 263.

[S11] H. Pfeiffer, F. Tancret and T. Brousse, *Electrochimica Acta*, **2005**, 50, 4763.

[S12] F. Poli, A. Wong, J. S. Kshetrimayum, L. Monconduit and M. Letellier, *Chemistry of Materials*, **2016**, 28, 1787.

[S13] S. Liu, Y. Qian and L. Xu, *Solid State Communications,* **2009**, 149, 438.

[S14] X. Wang, K. Han, Y. Gao, F. Wan and K. Jiang, *Journal of Crystal Growth*, **2007**, 307, 126.

[S15] H. Su, Y. Xie, B. Li, X. Liu and Y. Qian, *Solid State Ionics*, **1999**, 122, 157.

[S16] G. Manna, R. Bose and N. Pradhan, *Angewandte Chemie International Edition*,

2013, 52, 6762.

[S17] M. Fan, Y. Chen, Y. Xie, T. Yang, X. Shen, N. Xu, H. Yu and C. Yan, *Advanced Functional Materials*, **2016**, 26, 5019.

[S18] L. De Trizio, A. Figuerola, L. Manna, A. Genovese, C. George, R. Brescia, Z. Saghi, R. Simonutti, M. Van Huis and A. Falqui, *Acs Nano*, **2011**, 6, 32.

[S19] J. Liu, M. Meyns, T. Zhang, J. Arbiol, A. Cabot and A. Shavel, *Chemistry of Materials*, **2018**, 30, 1799.

[S20] S. Ni, J. Ma, X. Lv, X. Yang and L. Zhang, *Journal of Materials Chemistry A*, **2014**, 2, 20506.

[S21] B. M. Barry and E. G. Gillan, *Chemistry of Materials*, **2008**, 20, 2618.

[S22] B. M. Barry and E. G. Gillan, *Chemistry of Materials*, **2009**, 21, 4454.

[S23] F. Zhao, N. Han, W. Huang, J. Li, H. Ye, F. Chen and Y. Li, *Journal of Materials Chemistry A*, **2015**, 3, 21754.

[S24] M. Kong, H. Song and J. Zhou, *Advanced Energy Materials*, 2018, **8**, 1801489.

[S25] S. O. Kim and A. Manthiram, *Chemical Communications*, 2016, **52**, 4337.

[S26] S. Kaushik, J. Hwang, K. Matsumoto, Y. Sato and R. Hagiwara, *ChemElectroChem*, 2018, **5**, 1340-1344.

[S27] J. Li, X. Li, P. Liu, X. Zhu, R. N. Ali, H. Naz, Y. Yu and B. Xiang, *ACS Applied Materials & Interfaces*, 2019, **11**, 11442-11450.

[S28] Y. Von Lim, S. Huang, Y. Zhang, D. Kong, Y. Wang, L. Guo, J. Zhang, Y. Shi, T. P. Chen, L. K. Ang and H. Y. Yang, *Energy Storage Materials*, 2018, **15**, 98-107.

[S29] Y. Wang, Q. Fu, C. Li, H. Li and H. Tang, *ACS Sustainable Chemistry & Engineering*, 2018, **6**, 15083-15091.

[S30] F. Han, C. Y. J. Tan and Z. Gao, *ChemElectroChem*, 2016, **3**, 1054-1062.

[S31] X. Wang, K. Chen, G. Wang, X. Liu and H. Wang, *ACS Nano*, 2017, **11**, 11602-11616.

[S32] Z. Li, L. Zhang, X. Ge, C. Li, S. Dong, C. Wang and L. Yin, *Nano Energy*, 2017, **32**, 494-502.

[S33] D. Zhou and L.-Z. Fan, *Journal of Materials Chemistry A*, 2018, **6**, 2139-2147.

[S34] Y.-M. Xing, X.-H. Zhang, D.-H. Liu, W.-H. Li, L.-N. Sun, H.-B. Geng, J.-P. Zhang, H.-Y. Guan and X.-L. Wu, *ChemElectroChem*, 2017, **4**, 1395-1401.

[S35] X. Ge, Z. Li and L. Yin, *Nano Energy*, 2017, **32**, 117-124.

[S36] B. Wang, K. Chen, G. Wang, X. Liu, H. Wang and J. Bai, *Nanoscale*, 2019, **11**, 968-985.

[S37] W. Zhao, X. Ma, G. Wang, X. Long, Y. Li, W. Zhang and P. Zhang, *Applied Surface Science*, 2018, **445**, 167-174.

[S38] X.-W. Wang, H.-P. Guo, J. Liang, J.-F. Zhang, B. Zhang, J.-Z. Wang, W.-B. Luo, H.-K. Liu and S.-X. Dou, *Advanced Functional Materials*, 2018, **28**, 1801016.

[S39] J. Wang, B. Wang, X. Liu, G. Wang, H. Wang and J. Bai, *Journal of Colloid and Interface Science*, 2019, **538**, 187-198.

[S40] S. Shi, Z. Li, Y. Sun, B. Wang, Q. Liu, Y. Hou, S. Huang, J. Huang and Y. Zhao, *Nano Energy*, 2018, **48**, 510-517.

[S41] C. Dong, L. Guo, Y. He, C. Chen, Y. Qian, Y. Chen and L. Xu, *Energy Storage Materials*, 2018, **15**, 234-241.

[S42] C. Wu, P. Kopold, P. A. van Aken, J. Maier and Y. Yu, *Advanced Materials*, 2017, **29**.

[S43] H. Li, X. Wang, Z. Zhao, Z. Tian, D. Zhang and Y. Wu, *ChemElectroChem*, 2019, **6**, 404-412.

[S44] X. Miao, R. Yin, X. Ge, Z. Li and L. Yin, *Small*, 2017, **13**, 1702138.

[S45] S. Kaushik, K. Matsumoto, Y. Sato and R. Hagiwara, *Electrochemistry Communications*, 2019, **102**, 46-51.

[S46] D. Lan, W. Wang and L. Quan, *Nano Energy*, 2017, **39**, 506-512.

[S47] K.-W. Tseng, S.-B. Huang, W.-C. Chang and H.-Y. Tuan, *Chemistry of Materials*, 2018, **30**, 4440-4447.

[S48] Q. Pan, H. Chen, Z. Wu, Y. Wang, B. Zhong, L. Xia, H. Y. Wang, G. Cui, X. Guo and X. Sun, *Chemistry-A European Journal*, 2019, **25**, 971.

[S49] E. Pan, Y. Jin, C. Zhao, M. Jia, Q. Chang, R. Zhang and M. Jia, *Applied Surface Science*, 2019, **475**, 12-19.

[S50] X. Fan, T. Gao, C. Luo, F. Wang, J. Hu and C. Wang, *Nano Energy*, 2017, **38**, 350-357.

[S51] J. Liu, P. Kopold, C. Wu, P. A. van Aken, J. Maier and Y. Yu, *Energy & Environmental Science*, 2015, **8**, 3531-3538.

[S52] H. Sheng, M. Chao, X. Min, R. Shan and Y. Meng, *Sustainable Energy & Fuels*, 2017, **1**, 1944-1949.

[S53] L. Ma, P. Yan, S. Wu, G. Zhu and Y. Shen, *Journal of Materials Chemistry A*, 2017, **5**.

[S54] J. H. Choi, W. S. Kim, K. H. Kim and S. H. Hong, *Journal of Materials Chemistry A*, 2018, **6**, 17437-17443.

[S55] D. Lan, W. Wang, L. Shi, Y. Huang, L. Hu and Q. Li, *Journal of Materials Chemistry A*, 2017, **5**, 5791-5796.

[S56] Q. Li, Z. Li, Z. Zhang, C. Li, J. Ma, C. Wang, X. Ge, S. Dong and L. Yin, *Advanced Energy Materials*, 2016, **6**, 1600376.

[S57] H. S. Shin, K. N. Jung, Y. N. Jo, M. S. Park, H. Kim and J. W. Lee, *Scientific Reports*, 2016, **6**, 26195.

[S58] Y. Xu, B. Peng and F. M. Mulder, *Advanced Energy Materials*, 2018, **8**, 1701847.